Improved representation of phosphorus exchange on soil mineral surfaces reduces estimates of phosphorusP limitation in temperate forest ecosystems

Lin Yu[1,2], Silvia Caldararu[2,3], Bernhard Ahrens[2], Thomas Wutzler[2], Marion Schrumpf[2,4], Julian Helfenstein[5,6], Chiara Pistocchi[7], and Sönke Zaehle[2]

[1]Centre for Environmental and Climate Science, Lund University, Sölvegatan 37223 62 Lund, Sweden
[2]Max Planck Institute for Biogeochemistry, Hans-Knoell-Str. 10, Jena, 07745, Germany
[3]Department of Botany, Trinity College Dublin, Dublin, Ireland
[4]International Max Planck Research School (IMPRS) for Global Biogeochemical Cycles, Jena, 07745, Germany
[5]Agroscope, Reckenholzstrasse 191, 8046 Zürich, Switzerland
[6] Soil Geography and Landscape Group, Wageningen University, 6700 AA Wageningen, the Netherlands
[7] UMR Eco&Sols, Institut Agro Montpellier, CIRAD, INRAE, IRD, Place Viala 34060 Montpellier cedex 2, France

Lin Yu[1,2], Silvia Caldararu[2], Bernhard Ahrens[2], Thomas Wutzler[2], Marion Schrumpf[2,3], Julian Helfenstein[4,5], Chiara Pistocchi[65], and Sönke Zaehle[2]

[1]Centre for Environmental and Climate Science, Lund University, Sölvegatan 37223 62 Lund, Sweden
[2]Max Planck Institute for Biogeochemistry, Hans-Knoell-Str. 10, Jena, 07745, Germany
[3]International Max Planck Research School (IMPRS) for Global Biogeochemical Cycles, Jena, 07745, Germany
[4]Agroscope, Reckenholzstrasse 191, 8046 Zürich, Switzerland
[5] Soil Geography and Landscape Group, Wageningen University, 6700 AA Wageningen, the Netherlands
[6]UMR [5]Eco&Sols, Institut Agro Montpellier, CIRAD, INRAE, IRD, Place Viala 34060 Montpellier cedex 2, France

Correspondence to: Lin Yu (lin.yu@cec.lu.se)

Abstract. Phosphorus (P) availability affects the response of terrestrial ecosystems to environmental and climate change (e.g. elevated CO_2), yet the magnitude of this effect remains uncertain. This uncertainty arises mainly from a lack of quantitative understanding of the soil biological and geochemical P cycling processes, particularly the P exchange with soil mineral surfaces, which is often described by a Langmuir sorption isotherm.

We first conducted a literature review on P sorption experiments and terrestrial biosphere models (TBMs) using Langmuir isotherm. We then developed a new algorithm to describe the inorganic P exchange between soil solution and soil matrix based on the double-surface Langmuir isotherm and extracted empirical equations to calculate the sorption capacity and Langmuir coefficient. We finally tested the conventional and new models of P sorption at five beech forest sites in Germany along a soil P stock gradient using the QUINCY (QUantifying Interactions between terrestrial Nutrient CYcles and the climate system) TBM.

We found that the conventional (single-surface) Langmuir isotherm approach in most TBMs largely differed from P sorption experiments regarding the sorption capacities and Langmuir coefficients, and simulated a too low soil P buffering capacity. Conversely, the double-surface Langmuir isotherm approach adequately reproduced the observed patterns of soil inorganic P pools. The better representation of inorganic P cycling using the double Langmuir approach also improved simulated foliar N

and P concentrations, and the patterns of gross primary production and vegetation carbon across the soil P gradient. The novel model generally reduces the estimates of P limitation compared to the conventional model, particularly at the low-P site, as the model constraint of slow inorganic P exchange on plant productivity is reduced.

1 Introduction

Formatted: Font: (Default) +Headings (Times New Roma

40 Nutrient availability is one of the key factors affecting the productivity of terrestrial ecosystems and their future carbon (C) balance (Fernández-Martínez et al., 2014; Wieder et al., 2015). Although nitrogen (N) is the main constraint of plant biomass responses to elevated CO_2 (eCO2) concentration in many terrestrial ecosystems, phosphorus (P) availability likely constrains the biomass responses to eCO2 in major global biomes (Du et al., 2020; Elser et al., 2007; Lebauer and Treseder, 2008; Terrer et al., 2019). For instance, the tropical forests and forests grown on old soils are known to be strongly limited by P availability,

45 and might not be able to sequester additional C in the future as the CO_2 concentration continues to increase (Hubau et al., 2020; Jiang et al., 2020). While temperate and boreal forests are generally considered N limited (Lebauer and Treseder, 2008), recent studies have shown a decreasing P nutritional status is concomitant with increasing atmospheric CO_2 (Penuelas et al., 2020; Jonard et al., 2015). These findings highlight the importance of representing C-P interactions in terrestrial biosphere models (TBMs) and including P cycle processes in the future global C balance predictions.

50 There has been a continuous effort to include P cycling processes into TBMs in the past decade (Goll et al., 2012; Goll et al., 2017; Sun et al., 2020; Thum et al., 2019; Yang et al., 2014; Zhu et al., 2019; Wang et al., 2010; Yu et al., 2018). Many current TBMs employ the scheme (Fig.1a) developed by Wang et al. (2007) to describe soil geochemical processes. This model considers the soil inorganic P (Pi) as soluble Pi (P_{sol}), labile Pi (P_{lab}), sorbed Pi (P_{sorb}), occluded Pi (P_{ocl}) and primary Pi ($P_{primary}$), with few exceptions where labile and sorbed Pi pool are grouped into one pool (Zhu et al., 2019; Zhu et al., 2016). The

55 exchange between soil solution and soil matrix is described with a Langmuir adsorption isotherm assuming that P_{sol} quickly exchanges with P_{lab} on the mineral surface. The P_{lab} pool also slowly exchanges with P_{sorb} at a linear rate regardless of P_{sol} concentrations, but this relationship is parameterized very differently across TBMs (Helfenstein et al., 2020).

Many modelling studies emphasize the significance of biological P processes (Fleischer et al., 2019; Jonard et al., 2010; Yu et al., 2018; Wang et al., 2010) and ~~ignored~~underestimated the role of geochemical P processes~~., i.e. organic P recycling~~In these

60 models, ~~organic P recycling processes are the major fluxes, while the geochemical P fluxes are small~~in terrestrial ecosystems, ~~but the role of geochemical P processes is less discussed and remains unclear~~ (Sun et al., 2020). Particularly, the effect of (ad)sorption kinetics was seldom discussed in previous modelling studies (Fleischer et al., 2019; Yang et al., 2014), although they are known to directly and strongly regulate P_{sol} and P_{lab}, and thus affect P bioavailability (Frossard et al., 2000; Shen et al., 2011).

65 In this paper, we first conducted an extensive literature review of important soil characteristics affecting soil phosphorus sorption kinetics, and then developed ~~and applied~~ a ~~novel~~ model concept to reconcile measured P stocks with model simulations. In this new model, we applied the "two-surface" modification (Holford and Mattingly, 1976; Mcgechan and

Lewis, 2002) to the conventional single-surface Langmuir isotherm to formulate a novel algorithm for Pi exchange with mineral surfaces, namely double-surface Langmuir isotherm. We hypothesised that both P_{lab} and P_{sorb} exchange with P_{sol} in the new model (Fig. 1b), following the recent evidence from isotopic studies (Helfenstein et al., 2020; Frossard et al., 2011). We then compared and evaluated the performances of the novel and conventional models with measured soil Pi pools as well as foliar N and P concentrations for a gradient of soil P stocks (164–904 g P/ m^2) and availability in a similar climate (MAT 4.5–8 °C) and vegetation conditions (mature German beech forests, 120–140 yr). Lastly, we tested the sensitivity of the alternative Pi exchange schemes on ecosystem P and C cycling to changes in P cycling parameters, and tested the responses of them to changes in P availability (P fertilisation), C availability (CO$_2$ fertilisation), as well asand their combinationchanges in both P and C availability.

2 Methods

2.1 Literature review on Langmuir isotherm

The two parameters in Langmuir isotherm, maximum sorption capacity (S_{max}) and coefficient (K_m), are statistically fitted from measured adsorption curves of batch sorption experiments (Barrow, 1978). Following the scheme of Lloyd et al. (2001), most TBMs adapted the constant-equilibrium assumption to calculate a partition coefficient, k_p (Eq.2), which is the ratio of change in P_{sol} concentration to the change in available P (P_{sol} plus P_{lab}). The partition coefficient affects the rate of P_{sol} released from the P_{lab} pool as P_{sol} is consumed, thus eventually affects the soil P supply to plants and microbes.

$$P_{lab} = S_{max} \frac{P_{sol}}{K_m + P_{sol}} \tag{1}$$

$$k_p = \frac{\frac{dP_{sol}}{dt}}{\frac{dP_{sol}}{dt} + \frac{dP_{lab}}{dt}} = \frac{(P_{sol} + K_m)^2}{(P_{sol} + K_m)^2 + S_{max} K_m} \tag{2}$$

To better understand the characteristics of phosphate exchange between solution and soil mineral surface, we conducted a literature review of batch phosphate sorption experiments that describe the P sorption curves using Langmuir isotherm, and converted the fitted Langmuir parameters (Q_{max}, mg P/ kg soil, and K_L, L/ mg P, see Supplementary material Sect. S2) to sorption capacity and Langmuir coefficient and units commonly used in TBMs (S_{max} and K_m, g P/ m^2 in Eq.1). From the batch phosphate sorption experiments found in the literature, we calculated the partition coefficient (k_p) following Eq.2. Similarly, we reviewed the values of S_{max} and K_m in modelling studies and calculated k_p accordingly.

To showcase the difference of Langmuir isotherm parameter values in TBMs and experiments as well as the differences between single- and double-surface Langmuir isotherms, we compared the exchangeable soil Pi curves of different TBMs and, batch experiments data, to the double-surface Langmuir isotherm. We also simulated a desorption experiments with the single- and double-surface Langmuir isotherms to demonstrate their different responses to P removal.

2.2 QUINCY Model

QUINCY is a terrestrial biosphere model of coupled C, N, and P cycles as well as energy and water processes (Thum et al. 2019). The model represents the growth of vegetation and turnover of litter and soil organic matter at half-hourly timescales, coupled with the calculation of the terrestrial energy and water budgets. Vegetation is represented by average individuals of plant functional types (here a temperate broadleaved tree, see Section 2.3). Gross carbon uptake, leaf area and vegetation biomass and structure are directly influenced by nutrient availability through their effect on photosynthesis, tissue growth, allocation and mortality. The model explicitly considers depth profiles (discretized into 15 layers with a default total soil column depth of 9.5 m) of soil temperature, moisture and biogeochemical pools, representing litter and soil organic matter compartments, as well as inorganic forms of N and P. Vertical transport processes include diffusion and bioturbation. The phosphate exchange between soil solution and soil matrix is described using a conventional single-surface Langmuir isotherm, which is implemented the same way as in other TBMs. Different from other TBMs, QUINCY estimates S_{max} and K_m using soil texture and organic matter content (Thum et al. 2019).

To test our hypothesis that both P_{lab} and P_{sorb} exchange with P_{sol}, we modified the QUINCY Pi pool structure to describe the Pi exchange between solution and soil matrix (Fig.1b), using a double-surface Langmuir isotherm (Eq.3) (Holford & Mattingly 1976, McGechan & Lewis 2002).

$$P_{lab} = S_{max,1} \frac{P_{sol}}{K_{m,1}+P_{sol}} \tag{3.1}$$

$$P_{sorb} = S_{max,2} \frac{P_{sol}}{K_{m,2}+P_{sol}} \tag{3.2}$$

$$S_{max} = S_{max,1} + S_{max,2} \tag{3.3}$$

$$k_m = \frac{\frac{S_{max}}{hlp}-2P_{sol}\pm\sqrt{\frac{S_{max}^2}{hlp^2}-4\frac{S_{max}P_{sol}}{hlp}}}{2}, \tag{3.4}$$

where

$$hlp = \frac{S_{max,1}K_{m,1}}{(K_{m,1}+P_{lab})^2} + \frac{S_{max,2}K_{m,2}}{(K_{m,2}+P_{lab})^2} \tag{3.5}$$

The first sorption sites are responsible for the fast exchange (Eq. 3.1) between P_{sol} and P_{lab} and have much lower bonding strength than the second sorption sites that are responsible for the slower exchange (Eq. 3.2) between P_{sol} and P_{sorb}. We estimated two soil sorption maxima ($S_{max,1}$ and $S_{max,2}$, Eq. 3.3) and calculated two Langmuir coefficients ($K_{m,1}$ and $K_{m,2}$, Eqs. 3.4 and 3.5) based on batch experiments data from the literature review, assuming both single- and double-surface isotherms can be fitted with batch experiments data. Detailed derivation is described in Supplementary material Sect. S3.

2.3 Sites and data

We performed analysis at five mature beech forest stands in Germany, Bad Brückenau (BBR), Mitterfels (MTF), Vessertal (VES), Conventwald (COM), and Lüss (LUE]) (Table 1, Lang et al. 2017). Total soil P stocks (g P/m^2, up to 1 m depth) decrease strongly along the gradient: BBR (904) > MTF (678) > VES (464) > COM (231) > LUE (164).

Soil was sampled up to 1 m depth at each site, with layer depths of 5–10 cm, for the measurements of total C, N, and organic and inorganic P and other physio-chemical properties such as soil texture, pH, and oxalate-extractable Fe and Al. Modified Hedley fractionations (Tiessen and Moir (2008)) were conducted on soils from all depths for the measurements of labile Pi (P extractable with anionic resin and Pi extractable with 0.5 M NaHCO$_3$), sorbed Pi (Pi 0.1 M NaOH extractable Pi), occluded Pi (P residual (acid digestion)) and primary P (P 1 M HCl extractable P). Beech leaves were sampled in July/August from five trees for the measurements of leaf N and P concentrations.

2.4 Model setup, experiments, and evaluation

2.4.1 Model setup

To compare the performances of different phosphate exchange schemes, we applied here the conventional single-surface Langmuir isotherm (**siLang,** Fig.1a) as well as the novel double-surface Langmuir isotherm (**dbLang,** Fig. 1b) as model variants. To further test the causes for differences between these model variants, we introduced a **Control** simulation, which serves as a reference run without P limitation, and a **4pool** simulation (**4pool**, Fig. 1c), which serves as a special case of **siLang** that does not include slow Pi exchange. All four models employed Eq.3 to calculate the S_{max} and K_m in the Langmuir isotherms. In **siLang** and **4pool**, total sorption capacity (S_{max}, Eq.3.3) only refers to P_{lab} (or $P_{exchangeable}$), whereas in **dbLang** the two sorption maxima ($S_{max,1}$ and $S_{max,2}$) refers to P_{lab} and P_{sorb}, respectively. In the **Control** model, P_{sol} was kept at concentrations not limiting plant uptake or SOM decomposition. All models were initialized with a 15-layer soil column of 9.5 m which has a decreasing SOM content as soil depth increases (Thum et al., 2019). As for the inorganic P pools, the initial values of top 1 m soil were prescribed from the Hedley fractionation measurements and extrapolated to the deeper soil assuming an increased fraction of primary P and a decreasing fraction of exchangeable soil Pi pools (P_{lab} and P_{sorb}). The initialization of soil inorganic P pools deeper than 1 m is described in Supplementary material Sect. S4.

2.4.2 Model experiment protocol

The models were spun up for 500 years with meteorology and other atmospheric forcing (atmospheric CO_2, as well as N and P deposition), which are randomly drawn from the years from 1901 to 1930. During the model spinup, the P cycle was simulated dynamically, but the more stable Pi pools, i.e. P_{ocl}, and $P_{primary}$, were kept constant to ensure all the models initialized at the same field P status. After spinup, all models were run from 1901 to 2015 using the annual values for atmospheric CO_2, N (Lamarque et al., 2010; Lamarque et al., 2011) and P (Brahney et al., 2015; Chien et al., 2016) deposition, and the meteorology (Viovy, 2018) of the respective year. We used the same maximum biological N fixation rate for all study sites after calibration. The CN and CP ratios of the slow SOM pool were calibrated per site per soil depth to match the measured soil CN and CP ratios so that the simulated SOM cycling adequately represented the measured site condition. All the other parameter values were either taken from Thum et al.'s (2019) study or modified based on the development in this study, except for the maximum biological N fixation rate, which is set to be 2.5 kg N ha^{-1} yr^{-1} for all the study sites.

2.4.3 Model evaluation

Trend analyses were carried out with the Mann–Kendall test (M-K test) of the Kendall R package (Mcleod, 2011). In the Mann–Kendall test, the tau (τ) value varies between –1 and 1, where –1 represents a decreasing trend and 1 represents an increasing trend. The modeled soil profile against the measured soil profile was evaluated with a normalized root mean square ratio term, K_{nrmsr}, which is modified to represent the average proportions between modeled and measured values (Yu et al., 2020b).

$$K_{nrmsr} = \sqrt{\frac{\sum_1^n K_i^2}{n}}, where\ K_i = min\left(\frac{Mod_i}{Meas_i}, \frac{Meas_i}{Mod_i}\right) \tag{4}$$

K_i is the variable representing the ratio between simulated and measured values (in volumetric units) at the measured i_{th} layer. A paired t-test was conducted ~~between~~ on the K_{nrmsr} of all study sites between **siLang** and **dbLang** to verify if one model is statistically better than the other one.

2.5 Sensitivity analysis

To evaluate the response of alternative Langmuir isotherms to changes in P cycling processes, we further tested the sensitivity of the **siLang** and **dbLang** models to the P cycling parameterisation at one low-P site, Conventwald [COM], and one high-P site, Mitterfels [MTF], using a standard Latin hypercube design (LHS, Saltelli et al., 2004). We selected 16 parameters that directly control flux rates of inorganic or organic P cycling processes and varied each parameter by ±20% of its default value (Table S2) using LHS sampling of a uniform distribution, to form a set of 1000 LHS samples. The model outputs were evaluated in terms of GPP, foliar N and P contents, vegetation C stock, contents of SOC, total soil organic P (Po) and inorganic P, and ratio between P_{lab} and exchangeable Pi. We measured parameter importance as the rank-transformed partial correlation coefficients (RPCCs) to account for potential non-linearities in the association between model parameters and output (Zaehle et al., 2005; Saltelli et al., 2004).

2.6 Simulated CO2 and P fertilization experiments

To test the effects of phosphate exchange schemes to environmental changes, we conducted a CO_2 fertilization model experiment, a P fertilization model experiment, and a CO_2-P (CP) fertilization model experiment using **siLang**, **dbLang**, and **4pool** models at each study site. In the CO_2 fertilization experiment, the atmospheric CO_2 concentration was increased by 200 ppm from 2006 to 2015. In the P fertilization experiment, 50 kg/ha KH_2PO_4, i.e. 1139.7 mg P/m^2, was added once to the soil as soluble phosphate on September 16, 2006. The CP fertilization experiment is a combination of CO_2 and P fertilization experiments.

3 Results

3.1 Langmuir isotherm parameters in batch sorption experiments and TBMs

In batch sorption experiments, the maximum soil P sorption capacity S_{max} ranges from 187 to 829 g P/m^2 (25-quantile and 75-quantile values, median 390 g P/m^2) and the Langmuir coefficient K_m ranges from 0.21 to 4.5 g P/m^2 (median 0.93 g P/m^2), therefore the calculated partition coefficient k_p varies between 0.005 and 0.022 (median 0.01) (Table 2 and Fig. S1). Regarding the parameterization of S_{max} and K_m in TBMs, a few studies were directly retrieving values from sorption experiments (Wang et al., 2007; Yang et al., 2014), while most modeling studies estimate S_{max} and K_m based on soil types (Wang et al. 2010, Goll et al. 2012, Zhu et al. 2019) or soil texture (Thum et al. 2019).

The two studies using lab derived Langmuir parameters fitted well in the range of experimental values, but for those modeling studies that estimate Langmuir parameters, only the QUINCY model (Thum et al. 2019) produced reasonable Langmuir parameters and k_p values; while most other TBMs greatly overestimated K_m thus generating much higher k_p values than batch experiments (Table 2).

It is also shown in Fig. 2a that most TBMs are at or below the lower range of curves from batch sorption experiments data (BED) except the two isotherms from QUINCY that are close to the BED-median curve. All the other TBMs either have very low S_{max} or too high K_m, which can both lead to flattened soil Pi curves, indicating very low amounts of P are stored as exchangeable Pi in the soil even at high P_{sol} concentrations.

However, the responses to P removal are noticeably different between the single- and double-surface Langmuir (**siLang** and **dbLang**) given the similar soil Pi curves (Fig. 2b). The P_{sol} in **siLang** almost reached zero after a 30-day desorption experiment while the **dbLang** still maintained a P_{sol} level of 0.2 g/m^2, suggesting a much stronger buffering capacity in **dbLang** compared to **siLang**. This is mainly because the replenishing of P_{sol} in **siLang** is strongly limited by the rate of desorption from P_{sorb} to P_{lab}, but in **dbLang** the P_{sol} directly exchanges with P_{sorb} when the P is removed.

3.2 Simulated and measured ecosystem properties

The **siLang**, **dbLang**, and **4pool** models can adequately reproduce the measured SOC content, and SOM CN and CP ratios along soil profiles at all the study sites after site- and depth-specific calibration (Figs. 3a–c, Table S1). The performance of the three models did not differ much regarding the simulation of SOM profiles due to our calibration strategy (Tables 2 and S1). However, the novel **dbLang** model better reproduced the ratio between P_{lab} and exchangeable Pi (*Lab-to-Exchangeable P*) than **siLang** (K_{nrmsr} improvement 0.130±0.077, p < 0.05) (Table 3). The improvements of **dbLang** in modelling the labile (K_{nrmsr} improvement 0.030±0.147, p > 0.05) and sorbed Pi (K_{nrmsr} improvement 0.096±0.137, p > 0.05) pools were not as significant as that in modelling the *Lab-to-Exchangeable P* ratio (Table 3, Fig. 3d–f).

The simulated average foliar N content of four models (23.35±1.59, 23.05±1.84, 22.45±2.35, 22.74±2.27 mg N/g d.w. for **Control**, **dbLang**, **siLang**, and **4pool**, respectively) were within the average range of measured values (24.32±1.43 mg N/g d.w.). However, the simulated decreasing trend of foliar N content (M-K test, τ = -0.6, -0.8, -1, -0.8 for **Control**, **dbLang**,

siLang, and **4pool**, respectively) along the soil P gradient was not found in the measured data (M-K test, $\tau = -0.2$) (Fig. 4a). Decreasing trends in simulated foliar P content in all models (M-K test: $\tau = -0.8, -0.95, -1, -1$ for **Control**, **dbLang**, **siLang**, and **4pool**, respectively) were instead also seen in measurements, but the decreasing trend was much weaker (M-K test, $\tau = -0.6$) (Fig. 4b). The simulated foliar P content was highest in the **Control** model (1.40 ± 0.09 mg P/g d.w.) and lowest in **siLang**

220 (0.95 ± 0.21 mg P/g d.w.) at each study site, as **Control** is not P limited and the strongest P limitation occurs in **siLang**. The simulated difference in foliar P content across models is ~~more~~ a reflection of both ~~differing~~ plant P uptake ~~than~~ and productivity (Figs. 4 and S2–5). For example, at the P-rich BBR site, although the simulated gross primary productivity (GPP), leaf area index (LAI), aboveground C, and fine root C for the four models were almost identical (Fig. S2), the foliar P contents of four models ~~at the P-rich BBR site~~ were different due to differing plant P uptake ($0.99, 0.95, 0.89, 0.95$ g P/m^2/yr. for

225 **Control**, **dbLang**, **siLang**, and **4pool**, respectively; Fig. S24~~), the simulated gross primary productivity (GPP), leaf area index (LAI), aboveground C, and fine root C for the three models were almost identical (Fig. S2)~~. In contrast, at the P-poor LUE site, the differences among **siLang**, **dbLang** and **4pool** in GPP, LAI, and plant C were more pronounced than that in foliar P content, because ~~of~~ the ~~effect of limiting P availability~~limited P uptake ($0.67, 0.53, 0.55$ g P/m^2/yr. for **Control**, **dbLang**, and **siLang**, respectively; Fig. S2) ~~on plant growth~~ drastically changed the plant C allocation (e.g. leaf to root ratio) and led to the

230 subsequent changes in plant properties (Figs. 4 and S2).

3.3 Sensitivity analysis

Our sensitivity tests at the low-P COM site (231 g P/m^2) and the high-P MTF site (678 g P/m^2) showed a diverging effect of model choice and parameterization on selected ecosystem properties, such as GPP, plant C, and foliar P content (Figs. 5 and S6). Both models were very consistent in maintaining the vertical pattern of the simulated ratio between labile and

235 exchangeable Pi (*Lab-to-Exchangeable P*) across different parameterizations (Fig. S7). In other words, the better fit of **dbLang** in capturing the measured decreasing trend in *Lab-to-Exchangeable P* was robust against model parameters choice (Figs. S6 and S7).

The P cycling parameters with the strongest effect on the selected ecosystem properties were very different between the two models and moderately different between the two sites (Table S3 and Fig. 5). In **siLang**, the highest impacting parameters for

240 most selected outputs (e.g. ~~Foliar~~ foliar P, GPP, and plant C as in Fig. 5) was the absorption and desorption rate between P$_{lab}$ and P$_{sorb}$ (k_{abs} and k_{des}), i.e. the slow exchange process, while in **dbLang** they were the turnover rates and N: P ratios of slow and fast SOM pools (τ_{slow}, τ_{fast}, SOM_np, and microbial_np). One common feature for both models is that the low-P site, COM, was more affected by SOM_np, maximum weathering rate (k_weath_mineral) and maximum plant P uptake rate (vmax_uptake_p_p4) compared to the high-P site, MTF, inferring to a tighter P cycle in low-P ecosystem than high-P

245 ecosystem.

3.4 Modeled ecosystem responses to C, P, and CP fertilizations

The simulated ecosystem responses to CO_2 fertilization, P fertilization, and CP fertilization differed greatly among study sites, models, and fertilization types due to the differences in soil P availability and model schemes of Pi exchange (Figs. 6, 7, and S3–5). At the P-rich BBR site, the simulated GPP, LAI, aboveground and fine root C, plant uptake of N and phosphate increased after CO_2 and CP fertilizations, but did not change after P fertilization in all three models (**siLang**, **dbLang**, and **4pool**, Fig. 6a). It indicates that the simulations at BBR were not limited by P, which is also supported by the small difference of responses between CO_2 and CP fertilization experiments. In contrast, at the P-poor LUE site, the simulated responses to P and CP fertilization were much stronger than those after CO_2 fertilization in all three models (Fig. 6c), indicating a strong P limitation at LUE.

This simulated P stress among models can be quantified when compared to the **Control** model (Fig. 6d). The **siLang** model simulated the lowest plant P uptake at all three sites with high-, moderate- and low-P in soil. This difference in plant P uptake was only reflected in foliar P concentration at high-P site, but also reflected in other vegetation properties at moderate- to low-P sites. The **4pool** model, which is a special case of the single-surface Langmuir isotherm, simulated similar P stress to **dbLang** at high- and moderate-P sites, while at the low-P site, simulated a high P stress as **siLang** (Fig. 6d).

The changes of model P pools after CO_2, P, or CP fertilizations further illustrated the effects of Pi exchange schemes on ecosystem responses under varying soil P availability (Fig. 7). In the CO_2 fertilization experiment, the chronic increase of CO_2 led to increases in plant biomass P at all study sites in all three models (Fig. 7, top panel). The concurrent increases in plant P pools were compensated by decreases of labile and sorbed Pi as well as Po in the microbial (fast SOM) pool (fast SOM). At the high-P BBR site, the increases in plant P (631.4 ± 1.4 mg P/m^2), litter P (107.8 ± 0.8 mg P/m^2), slow Po in SOM (62.8 ± 0.3 mg P/m^2) were similar in all models, and the mobilization from soil exchangeable Pi (-417.4 ± 16.1 mg P/m^2) and fast Po SOM (-354.2 ± 2.5 mg P/m^2) contributed similarly as P sources. Conversely, at the P-poor LUE site, **dbLang** simulated a significantly higher plant P increase (188.3 mg P/m^2) than **siLang** (69.5 mg P/m^2) and **4pool** (18.5 mg P/m^2), due to its stronger capacity of mineralizing P from the microbial P pool. Because **dbLang** can maintain a much higher SOM pool in topsoil (Fig. 3a) as P_{sol} is better buffered under low soil Pi (Fig. 2b) compared to **siLang**, thus more P can be mineralized under eCO2.

In the P fertilization experiments, the fate of added P largely differed between **siLang** and **dbLang**, as the added P was preferably and quickly transferred to P_{sorb} in **dbLang** compared to **siLang** (Fig. 7, bottom panel).

In the CP fertilization (Fig. 7, middle panel), plant P did not gain more P at high- and moderate-P sites (BBR and VES) compared to the C fertilization, indicating both sites might not be P limited under eCO2. Surprisingly, microbes (fast SOM) also didn't benefit from P addition on top of eCO2 at BBR and VES, as most added P were was transferred to the soil Pi pools.

However, at the low-P LUE site (Fig. 7, last three columns), the combination of C and P fertilization produced higher plant P increases (928.5, 1202.3, and 971.1 mg P/m^2 for **4pool**, **dbLang** and **siLang**, respectively) than the P fertilization alone in all three models, inferring a very strong P limitation on C sequestration at the low-P LUE site.

4 Discussion

4.1 Model representation of soil Pi cycling and Langmuir sorption

280 The majority of terrestrial biosphere models (TBMs) describe the soil inorganic P (Pi) cycling processes with a similar structure of pools and fluxes (Figs. 1a or 1c), and mostly describe the key soil Pi exchange process, i.e. the (ad)sorption and desorption between soil solution and matrix, using the Langmuir isotherm. In this study, we have shown that the values of Langmuir parameters in most TBMs, namely maximum P sorption capacity (S_{max}, Eq.1) and half-saturation Langmuir coefficient (K_m, Eq.1), largely differ from those reported in the P sorption batch experiments (Table 2). This disagreement between TBMs and

285 experiments leads to much lower exchangeable soil Pi (P_{lab} plus P_{sorb}) contents in TBMs than experiments under the same soluble Pi (P_{sol}) (Fig. 2a). It is in line with the much higher partition coefficient (k_p, Eq.2) values in most TBMs than experiments (Table 2). Additionally, the reported S_{max} have a comparable size as the total soil Pi in experiments (Fig. S1), indicating that most of the soil-associated Pi could be exchanged with the soil solution at a certain point. This implies that the Langmuir isotherm can describe not only the fast exchange between P_{sol} and P_{lab} but also the slower exchange with P_{sorb}. This

290 hypothesis is supported by the classical sorption model of Barrow (Barrow, 1978, 1983) and the isotopic exchange kinetics conceptual model (Fardeau, 1995; Frossard and Sinaj, 1997; Morel et al., 2000) that Pi ions located in the soil matrix are distributed along a continuum of solubility, some being in rapid equilibrium with Pi ions in soil solution and some being in slow equilibrium.

Following the concept of the soil P solubility continuum, we have developed the double-surface Langmuir isotherm (**dbLang**,

295 Fig. 1b and Eq. 3) in the QUINCY TBM and parameterized it with the batch sorption experiments data. The double-surface Langmuir isotherm simulated a higher P buffering capacity than single-surface Langmuir isotherm (**siLang**) when P is removed from the soil (Fig. 2b), which is in agreement with the experimental results by Roberts and Johnston (2015). By comparing **dbLang** with the conventional **siLang** model and a special four-Pi-pool structure of **siLang** (**4pool** model, used in Zhu et al. 2016, 2019), we further investigated the effects of different sorption-desorption schemes on soil P under the QUINCY TBM

300 framework (Fig. 3). The model performance in simulating the relationship between soil labile and sorbed Pi pools (*Lab-to-Exchangeable P*) has been ~~greatly~~ improved by **dbLang** ~~(Figs. 3d–f, Table 3)~~ at our study sites of varying soil P stocks, soil texture and stoichiometry (Lang et al., 2017; Yu et al., 2020b). Such an improvement of **dbLang** in reproducing the *Lab-to-Exchangeable P* ratio is visually pronounced as it much better captures the vertical patterns of soil inorganic pools (Figs. 3d-f), it is also supported by statistical analysis that the measured soil P profiles were slightly better reproduced (Tables 3 and

305 S1). ~~The improvement~~This of **dbLang** ~~in reproducing the *Lab-to-Exchangeable P* ratio~~ was not simply caused by improvements in modelling the individual labile or sorbed Pi pool, but rather by a better ~~the improved~~ representation of the Pi exchange among P_{sol}, P_{lab}, and P_{sorb}, as such an improvement is independent of site conditions and model parameterization (Figs. 3 and S7). Additionally, the different performance of **siLang** and **dbLang** in this study shared the same set of parameters of QUINCY thus had the same model complexity. However, the new scheme did require more input than other TBMs in Table

310 2 as the new parameterizations were dependent on soil texture, pH, and extractable Al/Fe, while most other TBMs use prescribed values.

In this study, we have included the Hedley soil P data as part of the model validation, which, to our knowledge, has seldom been done before, although the Hedley soil P data (Yang and Post, 2011; Yang et al., 2013) have been widely used as initialization data for TBMs. The depth-explicit and quantitative evaluation of model Pi pools with field measurements
315 provides us a unique tool to diagnose different sorption-desorption schemes, and warrants future applications in model-data comparison or model -intercomparison studies.

4.2 Model performance and confidence

We have shown that **dbLang** performed better than **siLang** (and **4pool**) in reproducing the measured soil Pi pools and foliar P contents (Figs. 3 and 4, Table 3). Several ~~clues point toward~~observations suggest that the novel **dbLang** model produc~~iedng~~
320 more realistic patterns in GPP and vegetation C, although there is no direct evidence. First of all, Lang et al. (2017) have found that there are no trends in the measured tree heights or stand biomass along our soil P gradient (Table 1). Since all sites are unmanaged beech stands with a similar age structure, we can assume that GPP and vegetation C should also be similar between the sites in the absence of nutrient limitation. ~~It~~ This was better reproduced using **dbLang** than **siLang**, as less P limitation is simulated using **dbLang**. Secondly, studies have shown that biological processes dominate the C-P interactions in P-poor
325 beech forests (Bünemann et al., 2016; Pistocchi et al., 2018), which was ~~only~~ supported by the sensitivity results of only **dbLang** (Fig. 5 and Table S3). ~~w.~~ While in **siLang**, slow sorption/desorption process dominated GPP and vegetation C regardless of P availability. Most importantly, **siLang** overestimated P_{lab} and P_{sorb} in topsoil but still greatly underestimated the plant productivity and biomass at low-P sites (COM and LUE). Collectively, these findings suggest that a double Langmuir model of Pi sorption-desorption better described forest C and nutrient dynamics at these sites than the conventional single
330 Langmuir model.

Yang et al. (2014)~~'s study using~~ used the **siLang** scheme to study P cycling in P-limited tropical forests. ~~has also~~They show~~end~~ that a doubled rate of P transfer from P_{sorb} to P_{lab}~~,~~ leads to similar increases in plant productivity and biomass as a doubled P mineralization rate. This is in line with our sensitivity analysis of **siLang**, showing that slow sorption/desorption of P has similar impacts as SOM turnover on GPP and plant biomass (Fig. 5 and Table S3). However, this ~~, which~~ seems ~~also highly~~
335 ~~unrealistic~~ unlikely ~~at~~ in ~~Amazon~~ tropical forest sites ~~with~~ depleted in soil Pi, and we argue that a dbLang model could better capture such processes also in tropical forest ecosystems.

From the perspective of Pi cycling, the parameterization of linear P exchange between P_{lab} and P_{sorb} in **siLang** lacked clear foundations and experimental evidence, and hence largely differ among TBMs (Helfenstein et al. 2020). Similarly, we have shown that the exchange between P_{sol} and P_{lab} in most TBMs also largely ~~vary~~ varies and deviates from the reported ranges of
340 experiments (Table 2). Most importantly, the assumption that P_{sol} only exchanges with P_{lab} has been heavily questioned by experimentalists (Helfenstein et al. 2020, Morel et al. 2000) and it also differes from earlier models (Barrow, 1983; Devau et al., 2009; Van Der Zee and Gjaltema, 1992). The double-surface Langmuir isotherm much better represents the conceptual

sorption-desorption scheme that is supported by experimental data (Frossard et al., 2000; Frossard and Sinaj, 1997; Fardeau, 1995), and also implicitly considers some slower Pi exchange processes that are currently ignored in TBMs, such as chelation and dissolution/precipitation.

4.3 Ecosystem responses to perturbations

The different Pi sorption-desorption schemes have not only led to different simulated Pi pool sizes, but also caused varying ecosystem responses to elevated CO_2 and P addition (Figs. 6 and 7). The main difference between **siLang** and **dbLang** was the speed and extent of exchange between the soluble/labile and sorbed Pi pools. The added P was quickly transferred to the P_{lab} in both models, but the speed of Pi transfer to P_{sorb} was much faster in **dbLang**. ~~Because~~ This was because in **dbLang**, Pi directly transferred from P_{sol} to P_{sorb}, while in **siLang**, the transfer to P_{sorb} only occurred from P_{lab} and at a much slower rate. As a consequence, P_{sorb} in **dbLang** stored more P after P addition and it also released more P under higher CO_2 concentrations and elevated plant P demand. The fast transfer of P from P_{sol} to P_{lab} in both models is supported by evidence from ^{33}P tracer studies showing that the radioactivity of P_{sol} and P_{lab} converged quickly (< 3 months) after ^{33}P tracer addition (Pistocchi et al. 2018). However, the speed and extent of transfer to P_{sorb} cannot be easily confirmed with isotope signals since both ^{33}P and ^{32}P have ~~very~~ short half-lives ~~(Frossard et al. 2011)~~, but it is estimated to vary from days to weeks (Buehler et al., 2002; Helfenstein et al. 2021). Nevertheless, the mathematical and conceptual description of isotopic exchange kinetics tend to support the **dbLang** model, that the P transfer to P_{sorb} took place at a timescale of months rather than years in acidic soils (Bünemann et al. 2016, Frossard & Sinaj 1997, Helfenstein et al. 2020). Hou et al. (2019), using a data assimilation approach, also concluded that P transfer to P_{sorb} might happen at a much faster rate than the conventional TBM parameter values suggest.

Our advance in capturing soil Pi exchange has altered the responses of QUINCY to changing P availability, particularly at low-P sites. The main difference of soil Pi responses to P additions between **siLang** (also **4pool**) and **dbLang** is that the novel **dbLang** model can store or release more P from the sorbed Pi pool with a faster rate than **siLang**. Particularly, at sites with high P stress (e.g. LUE), a further increase in P stress (e.g. CO_2 fertilization) led to an increased P mineralization in **dbLang** rather than an increased P desorption in **siLang** (Fig. 7), as **dbLang** can establish a much larger (implicit) microbial ~~(fast SOM)~~ pool (fast SOM) in the topsoil to mineralize P (Fig. 3a). It was confirmed in the EucFACE experiment that both N and P mineralization increased by as much as 200% under eCO2 (Hasegawa et al., 2016). Additionally, evidence from isotopic studies has shown that biological processes, rather than geochemical processes, are dominant in both topsoil and subsoil of the P-poor LUE site (Pistocchi et al. 2018; Bünemann et al. 2016).

4.4 Limitation and future directions

The novel **dbLang** model much better represented soil Pi exchange and thus improved the C-P interactions in QUINCY, but there was a caveat when the P stress was high. At the P-poor site LUE, the GPP and vegetation C in **dbLang** were almost twice as high as those in **siLang** (Figs. S2a and S2c). However, such a huge release of P stress by **dbLang** was still not enough for LUE to reach similar plant productivity and biomass of BBR or VES, as indicated by field evidence (Lang et al. 2017). In

ecosystems with low soil P or high P stress, CO_2 fertilization enhances the organic P cycling processes, such as root exudation, phosphatase production, and microbial P mining (Ellsworth et al., 2017; Jiang et al., 2020; Lang et al., 2017; Pistocchi et al., 2020). Such responses in SOM cycling are not yet implemented in QUINCY, leading to a much lower GPP and plant biomass at low-P site than others. Nor were these mechanisms described in other TBMs, leading to poor model performance in low-P ecosystems, e.g. Amazon forests (Fleischer et al. 2019) and Eucalyptus forests (Medlyn et al. 2016). Recent developments in soil models/modules have endeavored to improve the model description of SOM cycling by including organo-mineral association process, explicit microbial dynamics, enzyme dynamics or allocation, mycorrhizal association, etc. (Huang et al., 2021; Yu et al., 2020a; Ahrens et al., 2020; Wutzler et al., 2017; Tang and Riley, 2014; Sulman et al., 2014; Wang et al., 2013). We believe that coupling novel **dbLang** scheme with a more mechanistic representation of SOM cycling will open the door to model the different forest ecosystem P cycling strategies (Lang et al. 2017) as well as to simulate the responses of low P ecosystems to elevated CO_2 (Jiang et al., 2020).

5 Conclusions

In this study, we first reviewed the implementation of the soil Pi exchange process in terrestrial biosphere models and compared the model implementations of P sorption with batch sorption experiment data. We found that the parameterizations used by most TBMs strongly underestimate the soil's P sorption capacity and overestimate the half-saturation Langmuir coefficient compared to the experimental data. In the QUINCY model, such a formulation leads to a much lower soil P binding capacity in TBMs than in reality, causing unrealistically large constraints of slow Pi exchange process on GPP and plant biomass, regardless of actual soil P availability. We presented a novel model scheme, based on a double-surface Langmuir isotherm, to describe the soil Pi exchange in better accordance with data from sorption experiments. This model parameterization better simulated the measured soil Pi pools and the GPP and plant C patterns of our study sites. It also better reproduced the topsoil SOM pools in the low-P site, therefore better simulating the responses of P pools/fluxes to elevated CO_2 than conventional TBMs. The novel double-surface Langmuir approach can thus serve as a better modelling tool to understand ecosystem response to global change.

References

Ahrens, B., Guggenberger, G., Rethemeyer, J., John, S., Marschner, B., Heinze, S., Angst, G., Mueller, C. W., Kögel-Knabner, I., Leuschner, C., Hertel, D., Bachmann, J., Reichstein, M., and Schrumpf, M.: Combination of energy limitation and sorption capacity explains 14C depth gradients, Soil Biology and Biochemistry, 148, 107912, https://doi.org/10.1016/j.soilbio.2020.107912, 2020.

Barrow, N. J.: The description of phosphate adsortion curves, Journal of Soil Science, 29, 447-462, 1978.

Barrow, N. J.: A mechanistic model for describing the sorption and desorption of phosphate by soil, Journal of Soil Science, 34, 733-750, 1983.

Barrow, N. J. and Shaw, T. C.: EFFECTS OF solUTION: SOIL RATIO AND VIGOUR OF SHAKING ON THE RATE OF PHOSPHATE ADSORPTION BY SOIL, Journal of Soil Science, 30, 67-76, https://doi.org/10.1111/j.1365-2389.1979.tb00965.x, 1979.

Brahney, J., Mahowald, N., Ward, D. S., Ballantyne, A. P., and Neff, J. C.: Is atmospheric phosphorus pollution altering global alpine Lake stoichiometry?, Global Biogeochemical Cycles, 29, 1369-1383, 10.1002/2015gb005137, 2015.

Buehler, S., Oberson, A., Rao, I. M., Friesen, D. K., and Frossard, E.: Sequential phosphorus extraction of a 33P-labeled oxisol under contrasting agricultural systems, Soil Science Society of America Journal, 66, 868-877, 2002.

Bünemann, E. K., Augstburger, S., and Frossard, E.: Dominance of either physicochemical or biological phosphorus cycling processes in temperate forest soils of contrasting phosphate availability, Soil Biology and Biochemistry, 101, 85-95, 10.1016/j.soilbio.2016.07.005, 2016.

Chien, C.-T., Mackey, K. R. M., Dutkiewicz, S., Mahowald, N. M., Prospero, J. M., and Paytan, A.: Effects of African dust deposition on phytoplankton in the western tropical Atlantic Ocean off Barbados, Global Biogeochemical Cycles, 30, 716-734, 10.1002/2015gb005334, 2016.

Devau, N., Cadre, E. L., Hinsinger, P., Jaillard, B., and Gérard, F.: Soil pH controls the environmental availability of phosphorus: Experimental and mechanistic modelling approaches, Applied Geochemistry, 24, 2163-2174, 10.1016/j.apgeochem.2009.09.020, 2009.

Du, E., Terrer, C., Pellegrini, A. F. A., Ahlström, A., van Lissa, C. J., Zhao, X., Xia, N., Wu, X., and Jackson, R. B.: Global patterns of terrestrial nitrogen and phosphorus limitation, Nature Geoscience, 13, 221-226, 10.1038/s41561-019-0530-4, 2020.

Ellsworth, David S., Anderson, Ian C., Crous, Kristine Y., Cooke, J., Drake, John E., Gherlenda, Andrew N., Gimeno, Teresa E., Macdonald, Catriona A., Medlyn, Belinda E., Powell, Jeff R., Tjoelker, Mark G., and Reich, Peter B.: Elevated CO2 does not increase eucalypt forest productivity on a low-phosphorus soil, Nature Climate Change, 7, 279-282, 10.1038/nclimate3235, 2017.

Elser, J. J., Bracken, M. E. S., Cleland, E. E., Gruner, D. S., Harpole, W. S., Hillebrand, H., Ngai, J. T., Seabloom, E. W., Shurin, J. B., and Smith, J. E.: Global analysis of nitrogen and phosphorus limitation of primary producers in freshwater, marine and terrestrial ecosystems, Ecology Letters, 10, 1135-1142, 10.1111/j.1461-0248.2007.01113.x, 2007.

Fardeau, J. C.: Dynamics of phosphate in soils. An isotopic outlook, Fertilizer Research, 45, 91-100, 10.1007/BF00790658, 1995.

Fernández-Martínez, M., Vicca, S., Janssens, I. A., Sardans, J., Luyssaert, S., Campioli, M., Chapin Iii, F. S., Ciais, P., Malhi, Y., Obersteiner, M., Papale, D., Piao, S. L., Reichstein, M., Rodà, F., and Peñuelas, J.: Nutrient availability as the key regulator of global forest carbon balance, Nature Climate Change, 4, 471, 10.1038/nclimate2177 https://www.nature.com/articles/nclimate2177#supplementary-information, 2014.

Fleischer, K., Rammig, A., De Kauwe, M. G., Walker, A. P., Domingues, T. F., Fuchslueger, L., Garcia, S., Goll, D. S., Grandis, A., Jiang, M., Haverd, V., Hofhansl, F., Holm, J. A., Kruijt, B., Leung, F., Medlyn, B. E., Mercado, L. M., Norby, R. J., Pak, B., von Randow, C., Quesada, C. A., Schaap, K. J., Valverde-Barrantes, O. J., Wang, Y.-P., Yang, X., Zaehle, S., Zhu, Q., and Lapola, D. M.: Amazon forest response to CO2 fertilization dependent on plant phosphorus acquisition, Nature Geoscience, 12, 736-741, 10.1038/s41561-019-0404-9, 2019.

Frossard, E. and Sinaj, S.: The Isotope Exchange Kinetic Technique: A Method to Describe the Availability of Inorganic Nutrients. Applications to K, P, S and Zn, Isotopes in Environmental and Health Studies, 34, 61-77, 10.1080/10256019808036360, 1997.

Frossard, E., Condron, L. M., Oberson, A., Sinaj, S., and Fardeau, J. C.: Processes governing phosphorus availability in temperate soils, Journal of Environmental Quality, 29, 15-23, 10.2134/jeq2000.00472425002900010003x, 2000.

Frossard, E., Achat, D. L., Bernasconi, S. M., Fardeau, J.-c., Jansa, J., Morel, C., Randriamanantsoa, L., Sinaj, S., and Oberson, A.: The Use of Tracers to Investigate Phosphate Cycling in Soil – Plant Systems, in: Phosphorus in Action Biological Processes in Soil Phosphorus Cycling, edited by: Bünemann, E., Oberson, A., and Frossard, E., Soil Biology, Springer Berlin Heidelberg, Berlin, Heidelberg, 59-91, 10.1007/978-3-642-15271-9, 2011.

Goll, D. S., Brovkin, V., Parida, B. R., Reick, C. H., Kattge, J., Reich, P. B., Van Bodegom, P. M., and Niinemets, Ü.: Nutrient limitation reduces land carbon uptake in simulations with a model of combined carbon, nitrogen and phosphorus cycling, Biogeosciences, 9, 3547-3569, 10.5194/bg-9-3547-2012, 2012.

Goll, D. S., Vuichard, N., Maignan, F., Jornet-Puig, A., Sardans, J., Violette, A., Peng, S., Sun, Y., Kvakic, M., Guimberteau, M., Guenet, B., Zaehle, S., Penuelas, J., Janssens, I., and Ciais, P.: A representation of the phosphorus cycle for ORCHIDEE (revision 4520), Geosci. Model Dev., 10, 3745-3770, 10.5194/gmd-10-3745-2017, 2017.

Hasegawa, S., Macdonald, C. A., and Power, S. A.: Elevated carbon dioxide increases soil nitrogen and phosphorus availability in a phosphorus-limited Eucalyptus woodland, Glob Chang Biol, 22, 1628-1643, 10.1111/gcb.13147, 2016.

Helfenstein, J., Pistocchi, C., Oberson, A., Tamburini, F., Goll, D. S., and Frossard, E.: Estimates of mean residence times of phosphorus in commonly considered inorganic soil phosphorus pools, Biogeosciences, 17, 441-454, 10.5194/bg-17-441-2020, 2020.

Holford, I. C. R. and Mattingly, G. E. G.: A model for the behaviour of labile phosphate in soil, Plant and Soil, 44, 219-229, 10.1007/BF00016969, 1976.

Hou, E., Lu, X., Jiang, L., Wen, D., and Luo, Y.: Quantifying Soil Phosphorus Dynamics: A Data Assimilation Approach, Journal of Geophysical Research: Biogeosciences, 124, 2159-2173, 10.1029/2018JG004903, 2019.

Huang, Y., Guenet, B., Wang, Y. L., and Ciais, P.: Global Simulation and Evaluation of Soil Organic Matter and Microbial Carbon and Nitrogen Stocks Using the Microbial Decomposition Model ORCHIMIC v2.0, 35, e2020GB006836, https://doi.org/10.1029/2020GB006836, 2021.

Hubau, W., Lewis, S. L., Phillips, O. L., Affum-Baffoe, K., Beeckman, H., Cuní-Sanchez, A., Daniels, A. K., Ewango, C. E. N., Fauset, S., Mukinzi, J. M., Sheil, D., Sonké, B., Sullivan, M. J. P., Sunderland, T. C. H., Taedoumg, H., Thomas, S. C., White, L. J. T., Abernethy, K. A., Adu-Bredu, S., Amani, C. A., Baker, T. R., Banin, L. F., Baya, F., Begne, S. K., Bennett, A. C., Benedet, F., Bitariho, R., Bocko, Y. E., Boeckx, P., Boundja, P., Brienen, R. J. W., Brncic, T., Chezeaux, E., Chuyong, G. B., Clark, C. J., Collins, M., Comiskey, J. A., Coomes,

465   D. A., Dargie, G. C., de Haulleville, T., Kamdem, M. N. D., Doucet, J.-L., Esquivel-Muelbert, A., Feldpausch, T. R., Fofanah, A., Foli, E. G., Gilpin, M., Gloor, E., Gonmadje, C., Gourlet-Fleury, S., Hall, J. S., Hamilton, A. C., Harris, D. J., Hart, T. B., Hockemba, M. B. N., Hladik, A., Ifo, S. A., Jeffery, K. J., Jucker, T., Yakusu, E. K., Kearsley, E., Kenfack, D., Koch, A., Leal, M. E., Levesley, A., Lindsell, J. A., Lisingo, J., Lopez-Gonzalez, G., Lovett, J. C., Makana, J.-R., Malhi, Y., Marshall, A. R., Martin, J., Martin, E. H., Mbayu, F. M., Medjibe, V. P., Mihindou, V., Mitchard, E. T. A., Moore, S., Munishi, P. K. T., Bengone, N. N., Ojo, L., Ondo, F. E., Peh, K. S. H.,

470   Pickavance, G. C., Poulsen, A. D., Poulsen, J. R., Qie, L., Reitsma, J., Rovero, F., Swaine, M. D., Talbot, J., Taplin, J., Taylor, D. M., Thomas, D. W., Toirambe, B., Mukendi, J. T., Tuagben, D., Umunay, P. M., van der Heijden, G. M. F., Verbeeck, H., Vleminckx, J., Willcock, S., Wöll, H., Woods, J. T., and Zemagho, L.: Asynchronous carbon sink saturation in African and Amazonian tropical forests, Nature, 579, 80-87, 10.1038/s41586-020-2035-0, 2020.

Jiang, M., Medlyn, B. E., Drake, J. E., Duursma, R. A., Anderson, I. C., Barton, C. V. M., Boer, M. M., Carrillo, Y., Castañeda-Gómez, L.,

475   Collins, L., Crous, K. Y., De Kauwe, M. G., dos Santos, B. M., Emmerson, K. M., Facey, S. L., Gherlenda, A. N., Gimeno, T. E., Hasegawa, S., Johnson, S. N., Kännaste, A., Macdonald, C. A., Mahmud, K., Moore, B. D., Nazaries, L., Neilson, E. H. J., Nielsen, U. N., Niinemets, Ü., Noh, N. J., Ochoa-Hueso, R., Pathare, V. S., Pendall, E., Pihlblad, J., Piñeiro, J., Powell, J. R., Power, S. A., Reich, P. B., Renchon, A. A., Riegler, M., Rinnan, R., Rymer, P. D., Salomón, R. L., Singh, B. K., Smith, B., Tjoelker, M. G., Walker, J. K. M., Wujeska-Klause, A., Yang, J., Zaehle, S., and Ellsworth, D. S.: The fate of carbon in a mature forest under carbon dioxide enrichment, Nature, 580, 227-231,

480   10.1038/s41586-020-2128-9, 2020.

Jonard, M., Augusto, L., Hanert, E., Achat, D. L., Bakker, M. R., Morel, C., Mollier, A., and Pellerin, S.: Modeling forest floor contribution to phosphorus supply to maritime pine seedlings in two-layered forest soils, Ecological Modelling, 221, 927-935, 10.1016/j.ecolmodel.2009.12.017, 2010.

Jonard, M., Fürst, A., Verstraeten, A., Thimonier, A., Timmermann, V., Potočić, N., Waldner, P., Benham, S., Hansen, K., Merilä, P.,

485   Ponette, Q., de la Cruz, A. C., Roskams, P., Nicolas, M., Croisé, L., Ingerslev, M., Matteucci, G., Decinti, B., Bascietto, M., and Rautio, P.: Tree mineral nutrition is deteriorating in Europe, Global Change Biology, 21, 418-430, 10.1111/gcb.12657, 2015.

Lamarque, J.-F., Kyle, G. P., Meinshausen, M., Riahi, K., Smith, S. J., van Vuuren, D. P., Conley, A. J., and Vitt, F.: Global and regional evolution of short-lived radiatively-active gases and aerosols in the Representative Concentration Pathways, Climatic Change, 109, 191, 10.1007/s10584-011-0155-0, 2011.

490   Lamarque, J. F., Bond, T. C., Eyring, V., Granier, C., Heil, A., Klimont, Z., Lee, D., Liousse, C., Mieville, A., Owen, B., Schultz, M. G., Shindell, D., Smith, S. J., Stehfest, E., Van Aardenne, J., Cooper, O. R., Kainuma, M., Mahowald, N., McConnell, J. R., Naik, V., Riahi, K., and van Vuuren, D. P.: Historical (1850–2000) gridded anthropogenic and biomass burning emissions of reactive gases and aerosols: methodology and application, Atmos. Chem. Phys., 10, 7017-7039, 10.5194/acp-10-7017-2010, 2010.

Lang, F., Krüger, J., Amelung, W., Willbold, S., Frossard, E., Bünemann, E. K., Bauhus, J., Nitschke, R., Kandeler, E., Marhan, S., Schulz,

495   S., Bergkemper, F., Schloter, M., Luster, J., Guggisberg, F., Kaiser, K., Mikutta, R., Guggenberger, G., Polle, A., Pena, R., Prietzel, J., Rodionov, A., Talkner, U., Meesenburg, H., von Wilpert, K., Hölscher, A., Dietrich, H. P., and Chmara, I.: Soil phosphorus supply controls P nutrition strategies of beech forest ecosystems in Central Europe, Biogeochemistry, 10.1007/s10533-017-0375-0, 2017.

LeBauer, D. S. and Treseder, K. K.: NITROGEN LIMITATION OF NET PRIMARY PRODUCTIVITY IN TERRESTRIAL ECOSYSTEMS IS GLOBALLY DISTRIBUTED, Ecology, 89, 371-379, https://doi.org/10.1890/06-2057.1, 2008.

500   Lloyd, J., Bird, M. I., Veenendaal, E. M., and Kruijt, B.: Should Phosphorus Availability Be Constraining Moist Tropical Forest Responses to Increasing CO2 Concentrations?, in: Global Biogeochemical Cycles in the Climate Systems, edited by: Schulze, E.-D., Heimann, M., Harrison, S., Holland, E., Lloyd, J., Prentice, I. C., and Schimel, D., Elsevier, New York, 95-114, 10.1016/b978-012631260-7/50010-8, 2001.

McGechan, M. B. and Lewis, D. R.: Sorption of Phosphorus by Soil, Part 1: Principles, Equations and Models, Biosystems Engineering, 82,

505   1-24, 10.1006/bioe.2002.0054, 2002.

McLeod, A. I.: Kendall Rank Correlation and Mann–Kendall Trend Test.R Package Version 2.2 [code], 2011.

Morel, C., Tunney, H., Plénet, D., and Pellerin, S.: Transfer of Phosphate Ions between Soil and Solution: Perspectives in Soil Testing, Journal of Environmental Quality, 29, 50-50, 10.2134/jeq2000.00472425002900010007x, 2000.

Penuelas, J., Fernández-Martínez, M., Vallicrosa, H., Maspons, J., Zuccarini, P., Carnicer, J., Sanders, T. G. M., Krüger, I., Obersteiner, M.,

510   Janssens, I. A., Ciais, P., and Sardans, J.: Increasing atmospheric CO2 concentrations correlate with declining nutritional status of European forests, Communications Biology, 3, 125, 10.1038/s42003-020-0839-y, 2020.

Pistocchi, C., Mészáros, É., Frossard, E., Bünemann, E. K., and Tamburini, F.: In or Out of Equilibrium? How Microbial Activity Controls the Oxygen Isotopic Composition of Phosphate in Forest Organic Horizons With Low and High Phosphorus Availability, 8, 10.3389/fenvs.2020.564778, 2020.

515   Pistocchi, C., Mészáros, É., Tamburini, F., Frossard, E., and Bünemann, E. K.: Biological processes dominate phosphorus dynamics under low phosphorus availability in organic horizons of temperate forest soils, Soil Biology and Biochemistry, 126, 64-75, https://doi.org/10.1016/j.soilbio.2018.08.013, 2018.

Roberts, T. L. and Johnston, A. E.: Phosphorus use efficiency and management in agriculture, Resources, Conservation and Recycling, 105, 275-281, 10.1016/j.resconrec.2015.09.013, 2015.

520 Saltelli, A., Tarantola, S., Campolongo, F., and Ratto, M.: Sensitivity analysis in practice: a guide to assessing scientific models, Wiley Online Library2004.

Shen, J., Lixing, Y., Junling, Z. H. L., Zhaohai, B., Xinping, C. W. Z., and Fusuo, Z.: Phosphorus Dynamics: From Soil to Plant, Plant Physiology, 156, 997-1005, 10.1104/pp.111.175232, 2011.

Sulman, B. N., Phillips, R. P., Oishi, A. C., Shevliakova, E., and Pacala, S. W.: Microbe-driven turnover offsets mineral-mediated storage
525 of soil carbon under elevated CO2, Nature Climate Change, 4, 1099, 10.1038/nclimate2436 https://www.nature.com/articles/nclimate2436#supplementary-information, 2014.

Sun, Y., Goll, D. S., Chang, J., Ciais, P., Guenet, B., Helfenstein, J., Huang, Y., Lauerwald, R., Maignan, F., Naipal, V., Wang, Y., Yang, H., and Zhang, H.: Global evaluation of nutrient enabled version land surface model ORCHIDEE-CNP v1.2 (r5986), Geosci. Model Dev. Discuss., 2020, 1-65, 10.5194/gmd-2020-93, 2020.

530 Tang, J. and Riley, W. J.: Weaker soil carbon–climate feedbacks resulting from microbial and abiotic interactions, Nature Climate Change, 5, 56, 10.1038/nclimate2438 https://www.nature.com/articles/nclimate2438#supplementary-information, 2014.

Terrer, C., Jackson, R. B., Prentice, I. C., Keenan, T. F., Kaiser, C., Vicca, S., Fisher, J. B., Reich, P. B., Stocker, B. D., Hungate, B. A., Peñuelas, J., McCallum, I., Soudzilovskaia, N. A., Cernusak, L. A., Talhelm, A. F., Van Sundert, K., Piao, S., Newton, P. C. D., Hovenden,
535 M. J., Blumenthal, D. M., Liu, Y. Y., Müller, C., Winter, K., Field, C. B., Viechtbauer, W., Van Lissa, C. J., Hoosbeek, M. R., Watanabe, M., Koike, T., Leshyk, V. O., Polley, H. W., and Franklin, O.: Nitrogen and phosphorus constrain the CO2 fertilization of global plant biomass, Nature Climate Change, 9, 684-689, 10.1038/s41558-019-0545-2, 2019.

Thum, T., Caldararu, S., Engel, J., Kern, M., Pallandt, M., Schnur, R., Yu, L., and Zaehle, S.: A new model of the coupled carbon, nitrogen, and phosphorus cycles in the terrestrial biosphere (QUINCY v1.0; revision 1996), Geosci. Model Dev., 12, 4781-4802, 10.5194/gmd-12-
540 4781-2019, 2019.

van der Zee, S. E. A. T. M. and Gjaltema, A.: Simulation of phosphate transport in soil columns. I. model development, Geoderma, 52, 87-109, 10.1016/0016-7061(92)90077-K, 1992.

Viovy, N.: CRUNCEP Version 7 - Atmospheric Forcing Data for the Community Land Model, Research Data Archive at the National Center for Atmospheric Research, Computational and Information Systems Laboratory [dataset], 10.5065/PZ8F-F017, 2018.

545 Wang, G., Post, W. M., and Mayes, M. A.: Development of microbial-enzyme-mediated decomposition model parameters through steady-state and dynamic analyses, Ecological Applications, 23, 255-272, 10.1890/12-0681.1, 2013.

Wang, Y. P., Houlton, B. Z., and Field, C. B.: A model of biogeochemical cycles of carbon, nitrogen, and phosphorus including symbiotic nitrogen fixation and phosphatase production, Global Biogeochemical Cycles, 21, 1-15, 10.1029/2006GB002797, 2007.

Wang, Y. P., Law, R. M., and Pak, B.: A global model of carbon, nitrogen and phosphorus cycles for the terrestrial biosphere,
550 Biogeosciences, 7, 2261-2282, 10.5194/bg-7-2261-2010, 2010.

Wieder, W. R., Cleveland, C. C., Smith, W. K., and Todd-Brown, K.: Future productivity and carbon storage limited by terrestrial nutrient availability, Nature Geoscience, 8, 441, 10.1038/ngeo2413 https://www.nature.com/articles/ngeo2413#supplementary-information, 2015.

Wutzler, T., Zaehle, S., Schrumpf, M., Ahrens, B., and Reichstein, M.: Adaptation of microbial resource allocation affects modelled long
555 term soil organic matter and nutrient cycling, Soil Biology and Biochemistry, 115, 322-336, https://doi.org/10.1016/j.soilbio.2017.08.031, 2017.

Yang, X. and Post, W. M.: Phosphorus transformations as a function of pedogenesis: A synthesis of soil phosphorus data using Hedley fractionation method, Biogeosciences, 8, 2907-2916, 10.5194/bg-8-2907-2011, 2011.

Yang, X., Post, W. M., Thornton, P. E., and Jain, A.: The distribution of soil phosphorus for global biogeochemical modeling,
560 Biogeosciences, 10, 2525-2537, 10.5194/bg-10-2525-2013, 2013.

Yang, X., Thornton, P. E., Ricciuto, D. M., and Post, W. M.: The role of phosphorus dynamics in tropical forests - A modeling study using CLM-CNP, Biogeosciences, 11, 1667-1681, 10.5194/bg-11-1667-2014, 2014.

Yu, L., Ahrens, B., Wutzler, T., Schrumpf, M., and Zaehle, S.: Jena Soil Model (JSM v1.0; revision 1934): a microbial soil organic carbon model integrated with nitrogen and phosphorus processes, Geosci. Model Dev., 13, 783-803, 10.5194/gmd-13-783-2020, 2020a.

565 Yu, L., Ahrens, B., Wutzler, T., Zaehle, S., and Schrumpf, M.: Modeling Soil Responses to Nitrogen and Phosphorus Fertilization Along a Soil Phosphorus Stock Gradient, Front. For. Glob. Change, 3, 543112, 10.3389/ffgc.2020.543112, 2020b.

Yu, L., Zanchi, G., Akselsson, C., Wallander, H., and Belyazid, S.: Modeling the forest phosphorus nutrition in a southwestern Swedish forest site, Ecological Modelling, 369, 88-100, https://doi.org/10.1016/j.ecolmodel.2017.12.018, 2018.

Zaehle, S., Sitch, S., Smith, B., and Hatterman, F.: Effects of parameter uncertainties on the modeling of terrestrial biosphere dynamics,
570 Global Biogeochemical Cycles, 19, 10.1029/2004GB002395, 2005.

Zhu, Q., Riley, W. J., Tang, J., and Koven, C. D.: Multiple soil nutrient competition between plants, microbes, and mineral surfaces: model development, parameterization, and example applications in several tropical forests, Biogeosciences, 13, 341-363, 10.5194/bg-13-341-2016, 2016.

Zhu, Q., Riley, W. J., Tang, J., Collier, N., Hoffman, F. M., Yang, X., and Bisht, G.: Representing Nitrogen, Phosphorus, and Carbon Interactions in the E3SM Land Model: Development and Global Benchmarking, Journal of Advances in Modeling Earth Systems, 11, 2238-2258, 10.1029/2018MS001571, 2019.

575

580
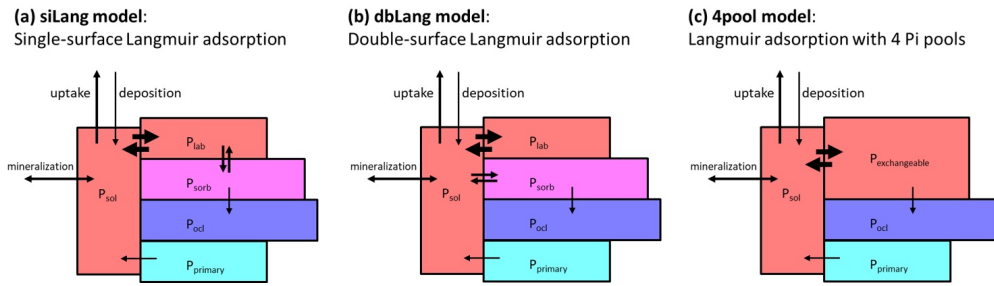
Figure 1: Model concept of (a) conventional Langmuir model (siLang), where only the labile P pool (P_{lab}) is exchanging P with the soil solution (P_{sol}) (b) double-surface Langmuir model (dbLang), where both P_{lab} and P_{sorb} are exchanging P with the soil solution but with different Langmuir parameters, and (c) a Langmuir model with only four inorganic P pools (4pool), where P_{lab} and P_{sorb}
585 **are combined to one pool, $P_{exchangeable}$, to which P_{sol} can get adsorbed via Langmuir sorption.**
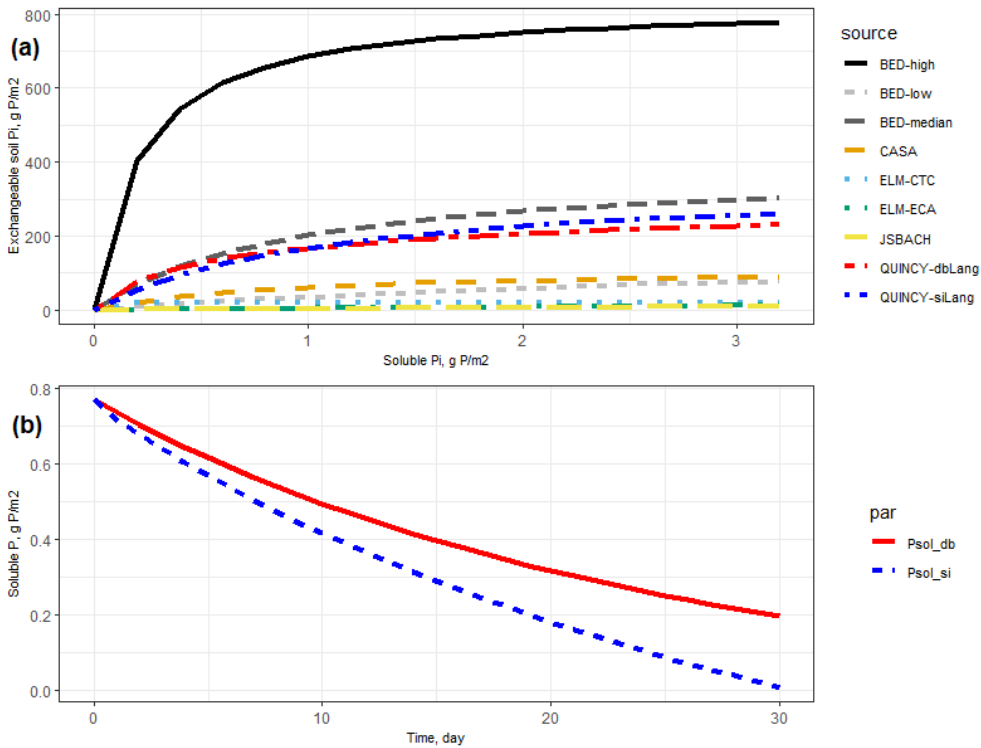
Figure 2: (a) Exchangeable soil inorganic P (P_{lab} plus P_{sorb}) curves based on different terrestrial biosphere models (TBMs) parameters and batch experiments data (BED). In TBMs, exchangeable soil Pi is defined as the sum of P_{lab} and P_{sorb}. In batch experiments data, soil exchangeable Pi only refers to P_{lab} in Eq. 1 due to a destructive experiment procedure which well mobilizes soil Pi (Barrow and Shaw, 1979). For conventional Langmuir model (siLang), P_{sorb} is calculated as 9/8 (global average ratio between P_{sorb} and P_{lab}, reported in Yang et al. 2013) of P_{lab} at all soluble P concentrations; for double-surface Langmuir model (dbLang), P_{sorb} is calculated following Eq. 3.2. (b) Simulated desorption curves for single- and double-surface Langmuir isotherms. The two desorption curves start with the same exchangeable soil Pi (152.2 g P/m², $P_{lab}+P_{sorb}$) and soluble Pi (0.769 g P/m², P_{sol}) contents, and the same amount of P (2.5 g P/m²) is removed from soil solution every day. Both Langmuir isotherms are assumed to be in equilibrium at a daily ~~timestep~~time step.
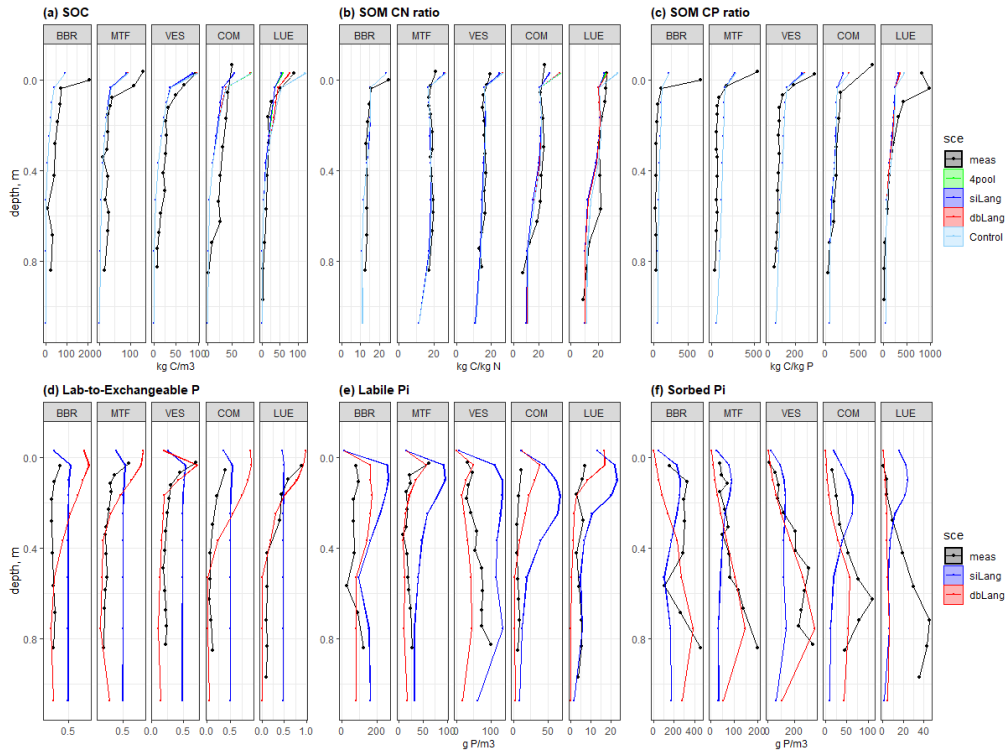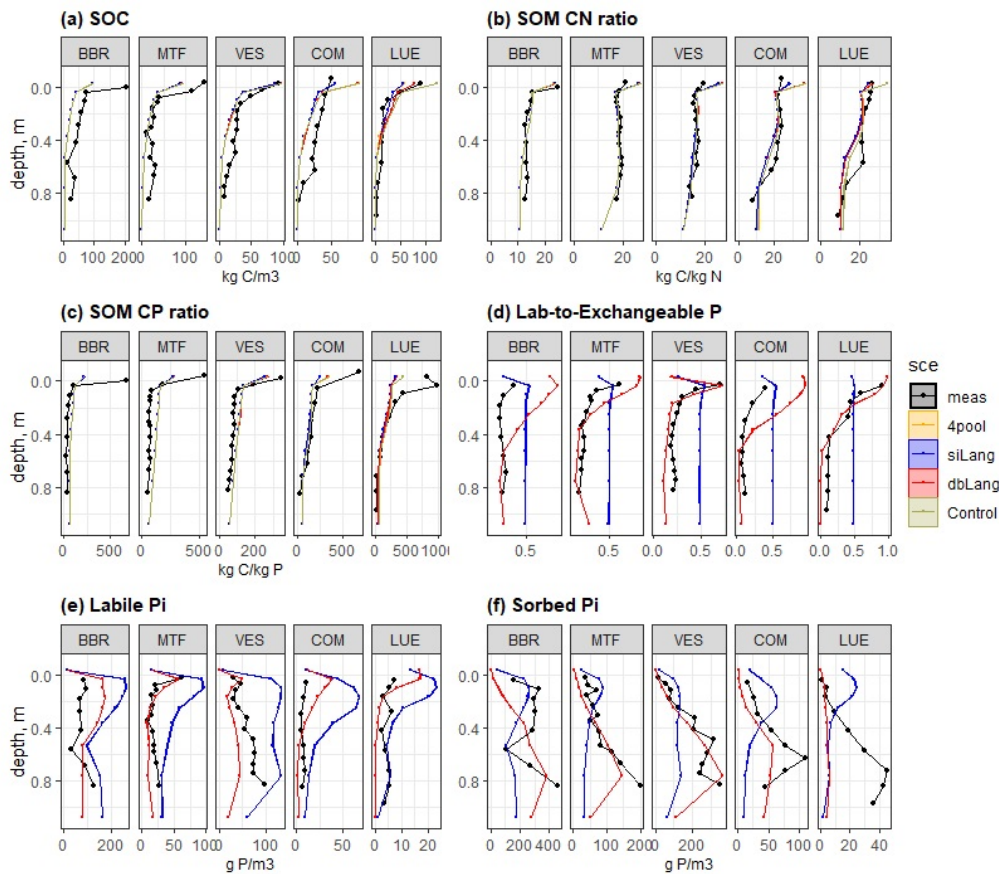
Figure 3: Simulated and measured (a) soil organic carbon (SOC), soil organic matter (SOM) (b) CN and (c) CP ratios, (d) ratio of labile to exchangeable Pi, (e) labile Pi, and (f) sorbed Pi of the study sites along the soil P availability gradient, BBR>MTF>VES>COM>LUE. The black dotted line is the field measurements, the ~~orange~~ lime line represents the Langmuir model with only four inorganic P pools (4pool), the blue line represents the single-surface Langmuir model (siLang), the red line represents the double-surface Langmuir model (dbLang), and the ~~dark yellow~~light sky-blue line represents the Control model. 4pool and Control are not applicable in (d), (e), and (f).

600
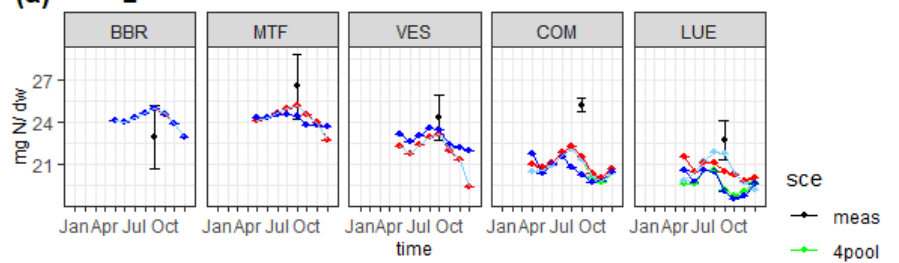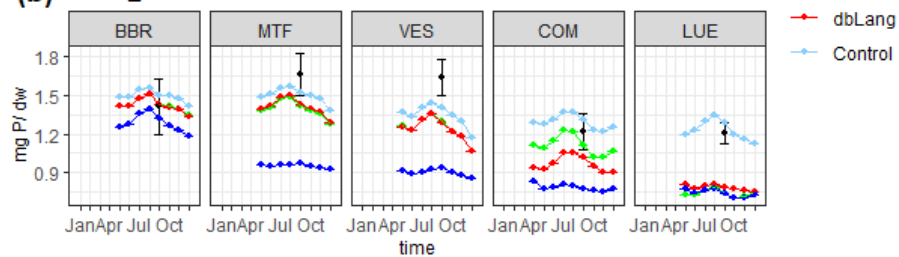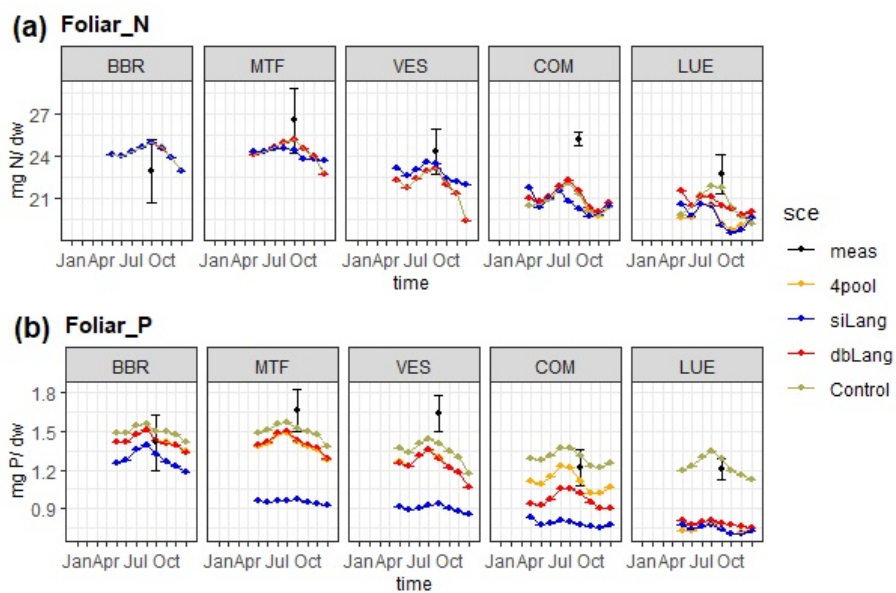
605

Figure 4: Simulated and measured foliar N (a) and P (b) contents along the soil P availability gradient. The simulated values are the yearly average of the period 2006–2015, and the measured values are sampled in 2014. The black dots are the field measurements, the ~~lime~~ orange line represents the Langmuir model with only four inorganic P pools (4pool), the blue line represents the single-surface Langmuir model (siLang), the red line represents the double-surface Langmuir model (dbLang), and the ~~dark yellow~~light sky-blue line represents the Control model.

610
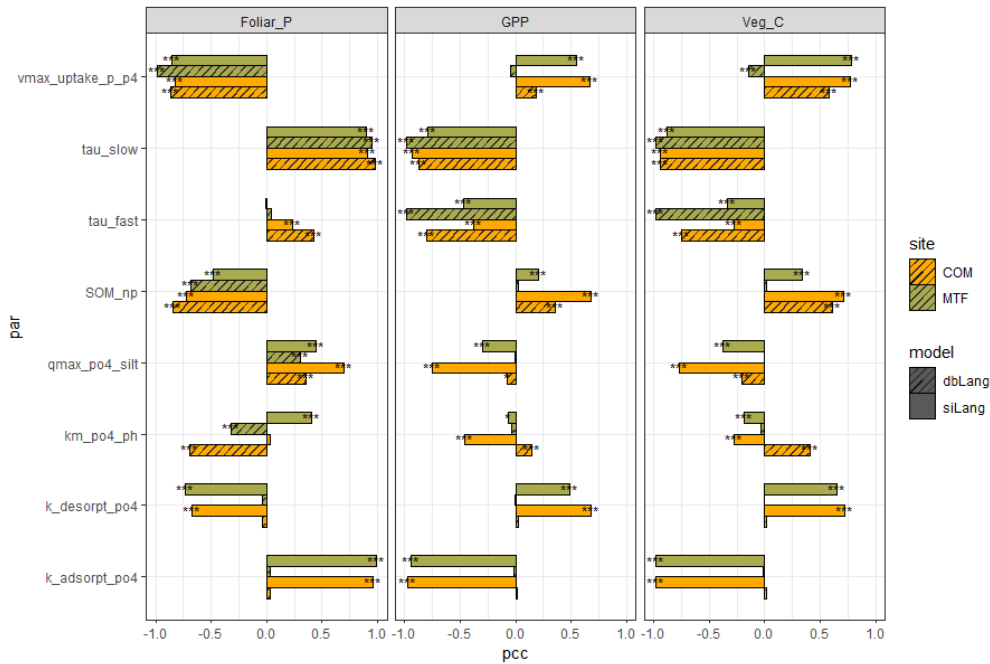
Figure 5: Partial correlation coefficient (pcc) values of eight main parameters on foliar P content, gross primary production (GPP) and vegetation C stock at COM and MTF sites of the single-surface Langmuir model (siLang) and the double-surface Langmuir model (dbLang) in the Latin hypercube design (LHS) sensitivity runs. The eight parameters are: maximum plant P uptake rate (vmax_uptake_p_p4), turnover rates of slow and fast soil organic matter (SOM) pools (tau_slow and tau_fast), N: P ratio of the slow SOM pool (SOM_NP), phosphate sorption capacity of fine soil (qmax_po4_silt), correction coefficient of pH on Langmuir K_m (km_po4_ph), and the absorption and desorption rate between P_{lab} and P_{sorb} (k_adsorpt_po4 and k_desorpt_po4). Significance level in figure: p<0.001 (***), p<0.01 (**), and p<0.05 (*).
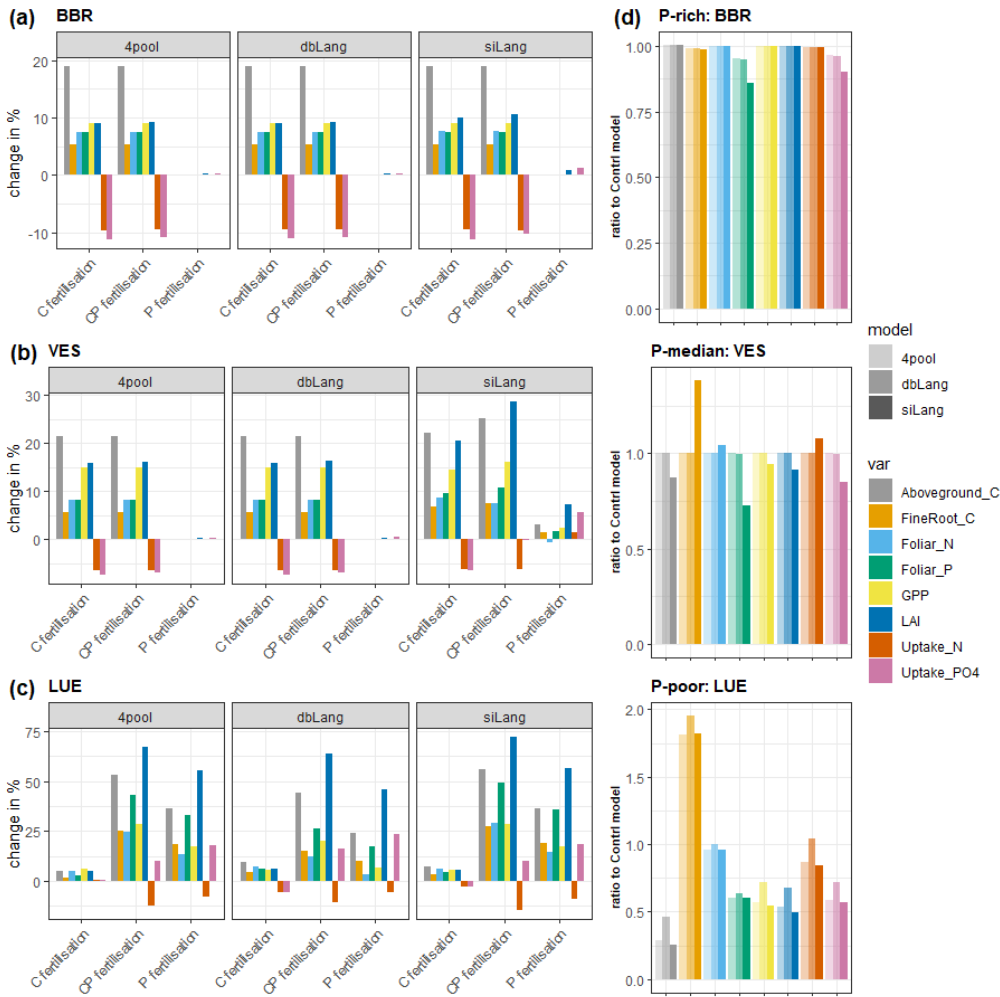
Figure 6: Simulated changes of gross primary production (GPP), aboveground C, fine root C, leaf area index (LAI), uptake of N and P, foliar N and P contents to CO_2, P, and CP fertilizations at (a) BBR, (b) VES, and (c) LUE sites and (d) the ratio of unfertilized scenarios of each model to the Control model. Bars are calculated as the changes in percentage in subplots (a) to (c), and bars in subplot (d) are fractions representing how much the models deviate from a non-P-limited condition.

625
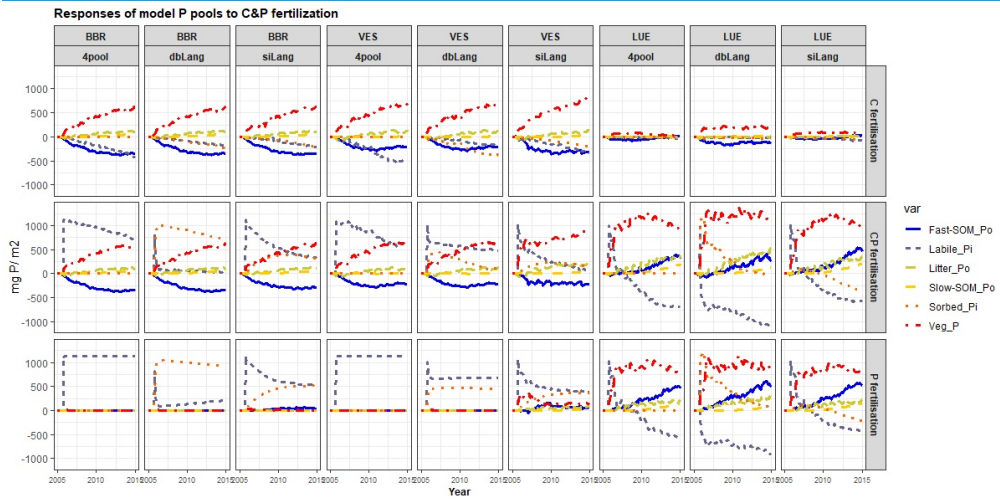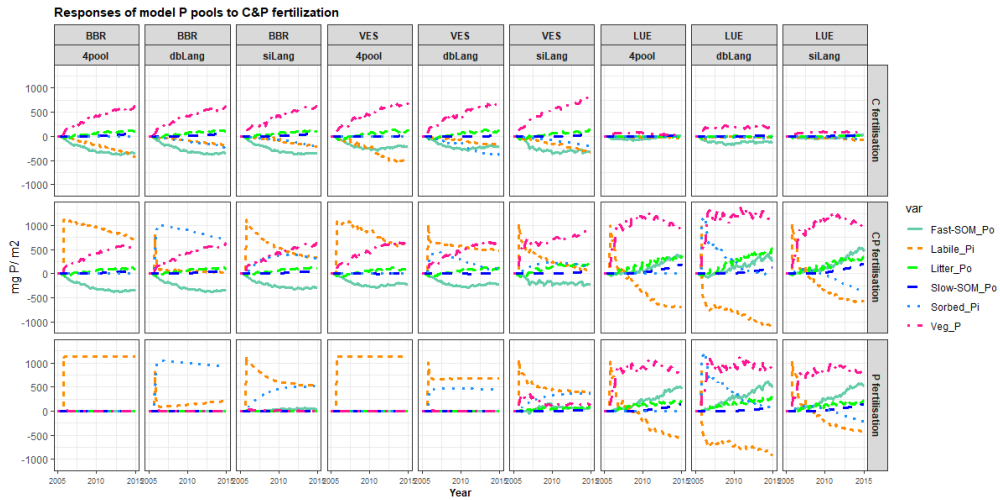
Figure 7: Simulated temporal responses of model P pools (labile Pi, sorbed Pi, litter Po, Po in fast and slow soil organic matter (SOM) pools [fast-SOM_Po and slow-SOM_Po], and P in the plant [Veg_P]) to CO_2, P, and CP fertilizations at BBR, VES, and LUE sites. In the C fertilization experiment, the atmospheric CO_2 concentration was increased by 200 ppm from 2006 to 2015. In the P fertilization experiment, 1139.7 mg P/m^2, was added once to the soil as soluble phosphate on Sep 16, 2006. The CP fertilization is the combination of C and P fertilizations. Each point in the x axis represents a P budget change at the specific time, with the size change of all P pools equal to zero (C fertilization) or the added P (1139.7 mg P/m^2, P and CP fertilization). The change of a specific P pool

630

at any given time equal to the total change of related P fluxes since the fertilization, e.g. plant P pool change relates to plant P uptake and P litterfall, labile Pi pool change relates to P adsorption (and P absorption) (Fig. 1), Po in fast SOM pool change relates to litter and fast SOM decomposition, and etc.

Study sites	BBR	MTF	VES	COM	LUE
Altitude (m a.s.l.)	809	1023	810	840	115
Mean annual temperature (°C)	5.8	4.5	5.5	6.8	8.0
Mean annual precipitation (mm)	1031	1299	1200	1749	779
Composition beech (*Fagus sylvatica* %)	*99*	*96*	*100*	*69*	*91*
Age *beeches* (a)	137	131	123	132	132
Height *beech* (mean basal area tree) (m)	26.8	20.8	29.3	27.6	27.3
Diameter at breast height *beeches*(cm)	36.8	37.6	40.1	39.9	27.5
Standing volume (m³ ha⁻¹)	495	274	550	685	529
Soil measurements in topsoil (0–30 cm) / subsoil (30–100 cm)					
Texture (topsoil) (WRB 2015)	Silty clay loam	Loam	Loam	Loam	Loamy sand
Texture (subsoil) (WRB 2015)	Loam	Sandy loam	Sandy loam	Sandy loam	Sand
Soil organic carbon (kg m⁻²)	18.7/17.6	14.2/13.1	12.9/8.2	13.1/8.8	8.9/5.4
Soil C:N	14.1/13.2	18.2/18.3	16.3/16.2	22.7/18.2	23.6/16.7
Soil N:P	3.6/2.4	5.1/3.3	6.2/4.4	8.5/5.7	16.5/3.7
P_{lab} (g m⁻²)	24.6/51.0	8.3/13.2	15.3/46.2	2.7/4.0	2.0/2.5
P_{sorb} (g m⁻²)	94.5/181.1	19.4/82.3	39.2/167.4	9.2/40.5	2.0/19.9

Table 2: Site characteristics of the study sites Bad Brückenau (BBR), Mitterfels (MTF), Vessertal (VES), Conventwald (COM), Lüss (LUE). Reproduced from Lang et al. (2017).

Model/Source	S_{max} (g/m²)	K_m (g/m²)	k_p	Reference
CASA-CNP	10 – 112	0.45 – 1.35	0.004 – 0.04	Wang et al. 2007
CABLE	91 ± 42	55 ± 23	0.40 ± 0.15	Wang et al. 2010

JSBACH	91 ± 36	60 ± 20	0.42 ± 0.13	Goll et al. 2012
ELM-CTC	10	0.00035 – 0.005	0.002 – 0.008	Yang et al. 2014
ELM-ECA	133	64	0.32	Zhu et al. 2016
ELMv1	91 ± 42	55 ± 23	0.40 ± 0.15	Zhu et al. 2019
ORCHIDEE-NP	NA		0.2 – 0.4	Goll et al. 2017
QUINCY	90 – 650	0.15 – 2	0.004 – 0.03	Thum et al. 2019
BED -mean	701 ± 11	6.7 ± 0.4	0.023 ± 7e-4	SI Ref. [1 – 27]
BED -25 quartile	187 ± 7	0.21 ± 0.14	0.005 ± 2e-4	SI Ref. [1 – 27]
BED -median	390 ± 15	0.93 ± 0.06	0.01 ± 3e-4	SI Ref. [1 – 27]
BED -75 quartile	829 ± 41	4.5 ± 0.4	0.022 ± 0.0015	SI Ref. [1 – 27]

Table 2: Maximum sorption capacity (S_{max}) and Langmuir coefficient (K_m) as well as the calculated partition coefficient (k_p) of phosphorus Langmuir (ad)sorption isotherm in TBMs and batch sorption experiments data (BED).

Soil profiles	K_{nrmsr} diff	p value
SOC	0.009±0.023	0.245
SOM CN ratio	0.005±0.005	0.059
SOM CP ratio	0.010±0.014	0.103
Bulk density	0.013±0.020	0.129
SOP	-0.016±0.018	0.919
SIP	0.058±0.051	**0.044***
Labile Pi	0.030±0.149	0.356
Sorbed Pi	0.096±0.137	0.118
Lab-to-Exchangeable P	0.130±0.077	**0.014***

640 **Table 3: Results for paired t-test between the normalized root mean square ratios (K_{nrmsr}, Table S1) of siLang and dbLang models of measured soil profile properties at all study sites. The null hypothesis is that dbLang performs no differently than siLang (i.e. dbLang has the same K_{nrmsr} values as siLang), and the hypothesis is rejected when the p value is smaller than 0.05 (values in bold with an asterisk).**

Acknowledgments

645 This work was supported by the Swedish government-funded Strategic Research Area Biodiversity and Ecosystems in a Changing Climate, BECC. SC was supported by the European Research Council (ERC) under the European Union's Horizon 2020 research and innovation programme (QUINCY; grant no. 647204). We are grateful to Prof. Dr. Friederike Lang, Jaane Krüger, and other co-workers from the German Research Foundation (DFG) funded priority research programme SPP1685 "Ecosystem Nutrition" for measuring and sharing the data, and to Dr. Jan Engel for technical assistance in developing the 650 code.

Author contributions

LY designed the study. LY and SZ formulated the paper outline. LY performed the literature review, model development, and analyses. SC, LY, and SZ developed the QUINCY model that forms the basis of the analysis in this manuscript. All authors contributed to writing the manuscript.

655 **Data availability**

The data in the literature review is available under request to the corresponding author.

Code availability

The scientific part of the code is available under a GPL v3 licence. The scientific code of QUINCY relies on software infrastructure from the MPI-ESM environment, which is subject to the MPI-M-Software-License-Agreement in its most recent 660 form (http://www.mpimet.mpg.de/en/science/models/license). The source code is available online (https://git.bgc-jena.mpg.de/quincy/quincy-model-releases), but its access is restricted to registered users. Readers interested in running the model should request a username and password from the corresponding authors or via the git-repository. Model users are strongly encouraged to follow the fair-use policy stated on https://www.bgc-jena.mpg.de/bgi/index.php/Projects/QUINCYModel.